EUROPEAN JOURNAL OF PURE AND APPLIED MATHEMATICS
2025, Vol. 18, Issue 4, Article Number 5803
ISSN 1307-5543 – ejpam.com
Published by New York Business Global

Chaotic and Quasi-Periodic Behaviors in Ferromagnetic Materials: A Dynamical Analysis Utilizing the Truncated Mittag-Leffler Function

Mostafa M. A. Khater[1,*]

[1] *Nonlinear Dynamics Research Center (NDRC), Ajman University, Ajman, UAE*

Abstract. This study conducts a thorough analysis of the nonlinear fractional complex Heisenberg ferromagnetic-type Akbota (FCHFA) model to clarify its dynamic behavior. Through rigorous bifurcation analysis, we identify stability transitions and determine critical parameter thresholds, revealing the system's sensitivity to perturbations. Employing advanced nonlinear dynamics techniques, we explore the fundamental mechanisms governing magnetization evolution. By integrating numerical simulations with analytical methods, we critically evaluate the role of fractional calculus in modeling long-range interactions and temporal memory effects in ferromagnetic systems.

The FCHFA model, which incorporates nonlinear spin-wave phenomena and phase transitions, offers a robust framework for analyzing magnetization dynamics. Numerically validated solutions confirm the effectiveness of our methodology, providing new insights into phase transitions and nonlinear wave phenomena. Our findings highlight the crucial role of fractional derivatives in capturing complex magnetization behaviors, thereby enhancing theoretical understanding and broadening the applicability of fractional models in condensed matter physics.

This work integrates fractional calculus with ferromagnetic theory, establishing a mathematically rigorous foundation for modeling systems with memory and nonlocal interactions. By rigorously validating numerical and analytical approaches, the study sets a precedent for investigating critical phenomena in fractional-order systems, with significant implications for device design in spintronics and magnetic materials. Furthermore, it demonstrates how fractional derivatives can effectively encapsulate the intricate dynamics of magnetization, including the interplay between memory effects and nonlinearity. By bridging theoretical developments with practical applications, this research not only advances the mathematical framework for studying complex magnetic materials but also opens avenues for innovative technological applications in the field of condensed matter physics.

2020 Mathematics Subject Classifications: 35Q51; 35C07; 82D30; 34K10.

Key Words and Phrases: Integrated approach; Fractional derivatives; Bifurcation analysis; Chaotic and quasi-periodic behaviors; Practical applications.

*Corresponding author.
DOI: https://doi.org/10.29020/nybg.ejpam.v18i4.5803

Email addresses: mostafa.khater2024@yahoo.com & khater@ajman.ac.ae (M. M. A. Khater)

1. Introduction

The exploration of fractional calculus applications in physics has unlocked novel avenues for investigating complex systems, especially in modeling magnetization and phase transitions within ferromagnetic materials. Ferromagnetic systems, governed by intricate nonlinear dynamics, display elaborate magnetization behaviors that fractional differential equations depict with superior efficacy compared to classical approaches [1]. The fractional complex Heisenberg ferromagnet-type Akbota (FCHFA) system emerges as a innovative methodology, furnishing enhanced insights into ferromagnetic characteristics by integrating fractional derivatives that encapsulate memory effects and anomalous diffusion [2]. Earlier studies on analogous fractional models have evidenced the capability of fractional calculus in portraying magnetization patterns and nonlinear wave propagation, laying a foundation for employing fractional techniques to investigate nonlinear evolution equations more broadly [3].

Despite the substantial advancements in fractional ferromagnetic models, a comprehensive comprehension of the magnetization dynamics and phase transitions within the FCHFA system remains incomplete. This study targets this knowledge lacuna by utilizing cutting-edge computational methodologies to scrutinize the solution architectures of the FCHFA system [4]. Our primary objectives are to deepen the understanding of the physical significance of fractional derivatives in ferromagnetic dynamics and to explore the broader implications for nonlinear wave propagation and phase transitions in condensed matter physics. Furthermore, this work endeavors to address fundamental questions surrounding the role of fractional calculus in providing a more precise description of magnetization dynamics than conventional methods [5].

The significance of this study resides in its contribution to the burgeoning field of fractional calculus and its application in condensed matter physics [6]. By probing the FCHFA system, this research unveils fresh insights into the mathematical depiction of magnetization and underscores the utility of fractional derivatives in capturing phenomena such as phase transitions, wave dispersion, and soliton propagation [7]. These discoveries not only enrich theoretical frameworks but also hint at potential applications in disciplines requiring precise modeling of ferromagnetic and nonlinear systems [8].

Numerous prior investigations have engaged with fractional Heisenberg and analogous ferromagnet-type systems, achieving remarkable progress in constructing soliton solutions and examining dynamical properties across diverse fractional forms [9]. While these studies have affirmed the relevance of fractional modeling in portraying ferromagnetic behaviors, they have been constrained by analytical limitations or the absence of high-precision computational techniques to evaluate solution robustness. By amalgamating the Khater II method, an enhanced Kudryashov approach, and the Adomian decomposition scheme, this study builds on previous work, offering a rigorous and innovative framework that surmounts prior constraints in accuracy and solution validation [10].

This research concentrates on the fractional complex Heisenberg ferromagnet-type Akbota system, a nonlinear evolution equation with profound physical implications for phase transitions and magnetization behaviors [11]. Nonlinear evolution equations akin to the FCHFA system play a pivotal role in transforming complex physical phenomena into mathematically tractable forms, particularly within condensed matter physics. Unlike other nonlinear evolution equations, the FCHFA system captures unique interactions and anisotropic attributes of ferromagnetic materials, distinguishing it from classical models. Its fractional nature permits a more nuanced representation of time-dependent behaviors, which are crucial for comprehending ferromagnetic dynamics at the microscopic level [12].

The mathematical framework of the FCHFA system is delineated as follows [13–15]:

$$\begin{cases} q\,\mathcal{D}_t^{\epsilon}\,\frac{\partial u}{\partial x} + p\,\frac{\partial^2 u}{\partial x\,\partial x} + i\mathcal{D}_t^{\epsilon}\,u + h\,u\,v = 0, \\ \\ \frac{\partial v}{\partial x} - 2\,\ell\,\left(q\,\mathcal{D}_t^{\epsilon}|u|^2 + p\,\frac{\partial |u|^2}{\partial x}\right) = 0, \end{cases} \tag{1}$$

where $u(x,t)$, $v(x,t)$, $|u|^2$ represent, respectively, the complex-valued transverse component of magnetization, the longitudinal component of magnetization, and the squared magnitude of the transverse magnetization.

In this investigation, we employ the truncated β-fractional derivative (symbolized as $\mathcal{D}_t^{\epsilon}$ in the main text and ${}_i\mathcal{D}_{\beta}^{\varepsilon,\vec{3}}$in the appendix) owing to its excellent capacity to model memory-dependent processes in magnetic systems. This selection is supported by the derivative's mathematical attributes, which effectively grasp non-local interactions and long-range correlations in ferromagnetic materials—phenomena that conventional derivatives struggle to represent accurately. The truncated β-fractional derivative offers a sturdy framework for dissecting the intricate temporal behaviors within our system, especially the memory effects that are vital for comprehending magnetization dynamics. A detailed elaboration of this derivative and its properties is furnished in Appendix 6.

The model comprises two equations, which can be physically interpreted as follows [16]:

(i) First equation's terms analysis:

- $q\,\mathcal{D}_t^{\epsilon}\left(\frac{\partial u}{\partial x}\right)$: Fractional time derivative of spatial change in transverse magnetization
- $p\,\frac{\partial^2 u}{\partial x^2}$: Spatial dispersion term (describing how magnetization spreads)
- $i\,\mathcal{D}_t^{\epsilon}u$: Fractional time evolution of transverse magnetization
- $h\,u\,v$: Coupling between transverse and longitudinal components

(ii) Second equation's terms analysis:

- $\frac{\partial v}{\partial x}$: Spatial variation of longitudinal magnetization
- $\mathcal{D}_t^{\epsilon}|u|^2$: Fractional time rate of change of magnetization intensity
- $\frac{\partial |u|^2}{\partial x}$: Spatial variation of magnetization intensity

Additionally, the physical meaning of the above-mentioned parameters in the FCHFA system (Eq. (1)) can be explained as follows

- q: Controls the strength of fractional time derivative effects
- p: Relates to the spatial dispersion strength
- h: Coupling coefficient between transverse and longitudinal components
- ℓ: Scaling parameter affecting the relationship between transverse and longitudinal components

The analyzed model (Eq. (1)) encapsulates vital physical attributes pertinent to nonlinear magnetic dynamics, particularly its capacity to depict the interaction between transverse and longitudinal magnetization components. By integrating the truncated β-fractional derivative, denoted as $\mathcal{D}^{\epsilon}$, $0 < \epsilon \leq 1$, the model accommodates memory effects and non-local interactions within the magnetic medium. The selection of this particular fractional derivative formulation stems from its preservation of key mathematical properties, such as the chain rule and product rule, while adeptly modeling the non-Markovian processes intrinsic to ferromagnetic systems. Distinct from alternative fractional derivatives, the truncated β-fractional derivative offers a more pragmatic mathematical framework that streamlines both analytical and numerical solutions, rendering it exceptionally fitting for our examination of complex magnetization dynamics. This configuration enables a coupling mechanism wherein alterations in transverse magnetization directly impact the longitudinal component and vice versa. Consequently, the model sustains diverse magnetic formations, including solitons and spin waves, mirroring a spectrum of potential dynamic behaviors within magnetic systems [17].

The physical relevance of this model is evident in its applicability to multiple complex phenomena in magnetic materials. It serves as a valuable tool for investigating magnetic domain dynamics, comprehending spin wave propagation, examining phase transitions in magnetization, and delineating non-local magnetic interactions [5]. Moreover, it facilitates the modeling of memory effects, which are of growing importance in the study of magnetic materials exhibiting intricate temporal behaviors [17].

Contrasted with classical Heisenberg models, the incorporation of fractional derivatives enhances this model's sophistication by encompassing long-range magnetic interactions and memory effects in magnetization dynamics. Additionally, it captures non-local spatial correlations, furnishing a framework for exploring anomalous diffusion processes in magnetic media. These improvements position this model as an advanced instrument

for probing the complex dynamics of magnetization in contemporary magnetic systems [5].

The study's methodology combines analytical and numerical techniques, leveraging the unique advantages of each approach. Specifically, the Khater II and enhanced Kudryashov methods are utilized to derive exact solutions, whereas the Adomian decomposition scheme evaluates the accuracy of these solutions, ensuring a thorough analysis of the system's complex behaviors [7, 8, 18, 19]. This dual approach offers an all-encompassing perspective on the FCHFA system, underscoring the precision of fractional calculus in capturing magnetization dynamics and soliton behavior. The results indicate that fractional derivatives are indispensable in detailing wave phenomena and soliton properties that prove challenging to model with conventional methods.

1.1. Memory Effects in the FCHFA Model

The memory effect is a fundamental characteristic of fractional-order systems that distinguishes them from their integer-order counterparts. In the context of our FCHFA model, this phenomenon manifests as the system's ability to retain information about its past states, allowing previous magnetization configurations to influence current and future dynamics. This section provides a detailed analysis of how memory effects emerge from the truncated β-fractional derivative formulation and their physical implications in ferromagnetic systems.

Mathematical Foundation of Memory Effects

The memory effect in our model is mathematically encoded through the truncated β-fractional derivative operator $\mathcal{D}_t^{\epsilon}$. Unlike conventional derivatives that depend only on local information, the truncated β-fractional derivative incorporates weighted contributions from all past states of the system. This non-local temporal dependence can be expressed mathematically as:

$$\mathcal{D}_t^{\epsilon} f(t) = \frac{t^{1-\epsilon}}{\Gamma(\mathfrak{Z}+1)} \frac{df(t)}{dt} \tag{2}$$

where $0 < \epsilon < 1$ and $\mathfrak{Z} > 0$. The factor $\frac{t^{1-\epsilon}}{\Gamma(\mathfrak{Z}+1)}$ serves as a weighting function that determines how strongly past states influence the current rate of change. As ϵ approaches 1, the memory effect weakens, and the system behavior approaches that of a conventional first-order derivative. Conversely, as ϵ decreases toward 0, the memory effect strengthens, causing the system to retain longer-term historical information.

Physical Manifestations of Memory in Ferromagnetic Systems

In ferromagnetic materials, memory effects manifest through several observable phenomena:

(i) **Hysteresis Behavior**: The magnetization of the material depends not only on the current external field but also on the history of field applications. This path-dependent behavior is naturally captured by our fractional model through terms like $q\,\mathcal{D}_t^{\epsilon}|u|^2$ in Eq. (1), which incorporate the historical evolution of magnetization intensity.

(ii) **Relaxation Dynamics**: When external fields are removed, ferromagnetic systems do not immediately return to equilibrium but instead follow complex relaxation patterns influenced by their magnetization history. The fractional time derivative terms in our model accurately reproduce these non-exponential relaxation processes.

(iii) **Spin-Wave Propagation**: The propagation of spin waves in ferromagnetic media exhibits dispersion characteristics that depend on the system's previous states. Our model captures this through the coupling of fractional time derivatives with spatial derivatives, as seen in the term $q\,\mathcal{D}_t^{\epsilon}\,\frac{\partial u}{\partial x}$ in Eq. (1).

Numerical Evidence of Memory Effects

To illustrate the impact of memory effects in our system, we conducted numerical simulations with varying fractional orders ϵ. For smaller values of ϵ (stronger memory), the system exhibits:

- Slower relaxation to equilibrium
- More pronounced hysteresis loops
- Enhanced stability against small perturbations
- Increased persistence of transient patterns

These characteristics are particularly evident in the evolution of the transverse magnetization component $u(x,t)$, where the fractional order ϵ directly modulates the temporal correlation length of the system.

Relationship Between Memory Effects and Long-Range Interactions

The memory effect in our fractional model is intrinsically connected to long-range interactions within the ferromagnetic medium. Conventional models based on integer-order derivatives implicitly assume that magnetic interactions are predominantly local, with each spin primarily influenced by its immediate neighbors. In contrast, our fractional approach acknowledges that in real ferromagnetic systems, each spin interacts with distant spins through various mechanisms, including dipole-dipole interactions and exchange coupling mediated by conduction electrons.

The truncated β-fractional derivative effectively captures these long-range interactions by introducing a power-law weighting of temporal correlations. This mathematical formulation aligns with experimental observations of non-Markovian dynamics in complex

magnetic systems, where the future evolution depends on the entire history rather than just the current state.

Implications for Phase Transitions and Critical Phenomena

Memory effects significantly influence phase transitions in ferromagnetic systems. Near critical points, conventional models often predict scaling behaviors that deviate from experimental observations. Our fractional approach addresses this limitation by incorporating memory effects that modify the critical exponents and scaling relations. The presence of memory in our model leads to:

- Modified critical temperatures that depend on the system's history
- Anomalous scaling of correlation functions near phase transitions
- History-dependent nucleation and growth of magnetic domains
- Non-universal critical behavior that varies with the fractional order ϵ

These features make our FCHFA model particularly valuable for studying complex ferromagnetic systems where conventional approaches fail to capture the full richness of observed behaviors.

In summary, the memory effect, mathematically encoded through the truncated β-fractional derivative, represents a fundamental aspect of our FCHFA model that enables more accurate representation of complex ferromagnetic phenomena. By explicitly accounting for the system's history dependence, our approach provides deeper insights into magnetization dynamics, phase transitions, and non-local interactions that are essential for understanding real ferromagnetic materials.

In this context, we implement the next wave transformation $u = \psi(\xi)\, e^{i(\frac{\kappa\,\Gamma(\varsigma+1)\,t^{\varepsilon}}{\varepsilon}+x)}$, $v = \psi(\xi)$, $\xi = \frac{\lambda\,\Gamma(\varsigma+1)\,t^{\varepsilon}}{\varepsilon}+x$ along with the truncated β–fractional derivative (For further information; see Appendix 6) on Eq. (1), where λ, κ are arbitrary constants to be determined later, leads to

$$\begin{cases} e^{i(\frac{\kappa\,\Gamma(\varsigma+1)\,t^{\varepsilon}}{\varepsilon}+x)}\,\left(-(\psi\,(-h\,\varphi+\kappa+p+\kappa\,q))+i\,\psi'(\lambda+2\,p+q\,(\kappa+\lambda))+\psi''\,(p+\lambda\,q)\right)=0, \\ \\ \varphi'-4\,\ell\,\psi\,\psi'(p+\lambda\,q)=0. \end{cases} \tag{3}$$

Separating the real and imaginary parts in the first equation of Eq. (3), yields

$$\begin{cases} \text{Re.} & \psi''(p+\lambda q)-\psi(-h\varphi+\kappa+p+\kappa q)=0, \\ \\ \text{Im.} & \psi'(\lambda+2p+q(\kappa+\lambda))=0. \end{cases} \tag{4}$$

By taking $\varphi = 2\psi^2\ell(p+\lambda q)$ and $\lambda = -2p - q(\kappa+\lambda)$, Eq. (3) converts into the next ordinary differential equation

$$\zeta_1\psi^3+\zeta_2\psi''+\psi=0, \tag{5}$$

where $\zeta_1 = \frac{2h\ell\left(p(2q-1)+q^2(\kappa+\lambda)\right)}{\kappa+p+\kappa q}$, $\zeta_2 = \frac{-2pq+p-\left(q^2(\kappa+\lambda)\right)}{\kappa+p+\kappa q}$. Balancing the highest order derivative term and nonlinear term in Eq. (5) along with the auxiliary equations of the suggested analytical scheme

$$\begin{cases} \text{Khat II method's auxiliary equation} & \begin{cases} \phi'(\xi) \to -f(\xi)\phi(\xi), \\ f'(\xi) \to -\delta - f(\xi)^2, \end{cases} \\ \text{EKud method's auxiliary equation} & f''(\xi) \to f(\xi) - 2\,\tau\, f(\xi)^3, \end{cases} \tag{6}$$

where, δ, τ are arbitrary constants to be determined later., yield constructing the general solutions of Eq. (5) in the next form

$$\psi(\xi) = \begin{cases} \sum_{i=1}^{n} \left(a_i\, f(\xi)^i + b_i\, \phi(\xi)\, f(\xi)^{i-1}\right) + a_0, & \text{Khat II method's Sol.}, \\ \sum_{i=1}^{n} \left(a_i f(\xi)^i + b_i \left(\frac{f'(\xi)}{f(\xi)}\right)^i\right) + a_0, & \text{EKud method's Sol.}, \end{cases} \tag{7}$$

where $n = 1$, while a_i, b_i are arbitrary constants to be determined later.

The structure of this paper is organized as follows:

Commencing with Section 2, we carry out an extensive exploration of the model's dynamical properties via bifurcation analysis, examination of chaotic and quasi-periodic behaviors, and evaluation of sensitivity to parameter variations. Our goal is to clarify the fundamental mechanisms governing the system's evolution by employing advanced mathematical tools from nonlinear dynamical theory.

In Section 3, we conduct a thorough review of the analytical and numerical methods utilized to derive solutions for the studied model.

Section 4 offers comprehensive numerical simulations that shed light on the dynamics of the model's solutions, providing deep insights into its associated physical properties. Section 5 elaborates on the scientific contributions of this work, emphasizing the unique features and significance of the derived solutions.

Finally, Section 6 delivers concluding remarks, summarizing the main findings and their implications, and synthesizes the research conducted.

2. Dynamical Analysis of the FCHFA Model

This investigation delves into the nonlinear FCHFA model, focusing on its dynamical properties through bifurcation analysis, exploration of chaotic and quasi-periodic behaviors, and assessment of sensitivity to parameter variations. The primary objective is to employ advanced mathematical tools from nonlinear dynamical theory to uncover the fundamental mechanisms governing the system's evolution.

2.1. Bifurcation Analysis

The bifurcation analysis involves examining the phase-space trajectories of the planar dynamical system derived from the Riemann coupled wave equation. By applying a Galilean transformation to the original equation, the system can be expressed in its canonical form as:

$$\begin{cases} \dfrac{d\psi}{d\mathfrak{T}} = \upsilon, \\ \\ \dfrac{d\upsilon}{d\mathfrak{T}} = -\dfrac{\zeta_1\,\psi^3}{\zeta_2} - \dfrac{\psi}{\zeta_2}. \end{cases} \tag{8}$$

This system allows for the characterization of the traveling wave solutions based on the principles of planar dynamical systems. The Hamiltonian function associated with the system is given by:

$$\mathcal{H}(\psi,\upsilon) = \frac{2\,\zeta_2\,\upsilon^2 + \zeta_1\,\psi^4 + 2\,\psi^2}{4\,\zeta_2} = \mathcal{G}, \tag{9}$$

where $\mathcal{H}(\psi,\upsilon)$ represents the total energy of the system, comprising the kinetic energy term $(\frac{\upsilon^2}{2})$ and the potential energy term $\left(\frac{\zeta_1\,\psi^4+2\,\psi^2}{4\,\zeta_2}\right)$.

Equilibrium Points

The equilibrium points of the system are determined by setting $\left(\frac{d\psi}{d\mathfrak{T}} = 0\right)$ and $\left(\frac{d\upsilon}{d\mathfrak{T}} = 0\right)$, which leads to:

$$\begin{cases} \upsilon = 0, \\ \\ \dfrac{\zeta_1\,\psi^3}{\zeta_2} + \dfrac{\psi}{\zeta_2} = 0. \end{cases} \tag{10}$$

The solutions to (10) yield the equilibrium points $E_1 = (0,0)$, $E_2 = \left(-\frac{i}{\sqrt{\zeta_1}},0\right)$, and $E_3 = \left(\frac{i}{\sqrt{\zeta_1}},0\right)$.

Stability Analysis

To assess the stability of the equilibrium points, we compute the Jacobian matrix $\mathcal{J}(\psi,\upsilon)$ for the system (8):

$$\mathcal{J}(\psi,\upsilon) = \begin{pmatrix} 0 & 1 \\ -\frac{3\,\zeta_1\,\psi^2+1}{\zeta_2} & 0 \end{pmatrix}. \tag{11}$$

The determinant of $\mathcal{J}(\psi, \upsilon)$ is:

$$\det(\mathcal{J}(\psi, \upsilon)) = \frac{3\,\zeta_1\,\psi^2 + 1}{\zeta_2}. \tag{12}$$

The stability of the equilibrium points depends on the eigenvalues of $\mathcal{J}(\psi, \upsilon)$. These eigenvalues are obtained by solving the characteristic equation:

$$\det(\mathcal{J}(\psi, \upsilon) - \lambda I) = \det\left(\begin{pmatrix} 0 & 1 \\ -\frac{3\,\zeta_1\,\psi^2+1}{\zeta_2} & 0 \end{pmatrix} - \lambda \begin{pmatrix} 1 & 0 \\ 0 & 1 \end{pmatrix}\right) = 0. \tag{13}$$

This simplifies to:

$$\det\begin{pmatrix} -\lambda & 1 \\ -\frac{4\,\eta+\kappa\,\lambda^3+12\,\lambda\,\psi}{\lambda} & -\lambda \end{pmatrix} = 0. \tag{14}$$

Simplifying this expression:

$$\lambda^2 - \frac{3\,\zeta_1\,\psi^2 + 1}{\zeta_2} = 0. \tag{15}$$

At this point, solving the cubic equation is necessary. The roots of the equation give the eigenvalues of the matrix $\mathcal{J}(\psi, \upsilon)$.

The eigenvalues of a matrix reveal key aspects of the system it represents. In this case, the eigenvalues are real and have opposite signs, suggesting the presence of a saddle point, where some solutions grow while others decay. The magnitude of the eigenvalues indicates the rate of growth or decay, with larger values leading to faster dynamics. Since the eigenvalues are not complex, the system does not exhibit oscillatory behavior but instead evolves monotonically in different directions. The eigenvalues thus provide insights into the stability of the system, with positive eigenvalues indicating instability and negative ones suggesting stable dynamics along certain directions. Understanding these eigenvalues helps in predicting how the system will behave over time, whether it will stabilize or diverge.

The analysis reveals that the nature of the equilibrium points varies significantly with the parameter values (ζ_1, ζ_2), as summarized below:

- For $(\zeta_1, \zeta_2) = (-4, -2)$, E_1 is a saddle point, and E_2, E_3 are center points.
- For $(\zeta_1, \zeta_2) = (-9, 2)$, E_1 is a center point, and E_2, E_3 are a saddle points.

The bifurcation diagrams in Figure 1 illustrate these scenarios, showcasing the significant influence of parameter variations on the system's dynamics.

2.2. Chaotic and Quasi-Periodic Dynamics

To investigate the chaotic dynamics, a perturbation term of the form $\mathfrak{Z}\cos(\Upsilon\mathfrak{T})$ is introduced into the system, yielding the modified equations:

$$\begin{cases} \dfrac{d\psi}{d\mathfrak{T}} = \upsilon, \\ \\ \dfrac{d\upsilon}{d\mathfrak{T}} = -\dfrac{\zeta_1\,\psi^3 + \psi}{\zeta_2} + \mathfrak{Z}\,\cos(\Upsilon\,\mathfrak{T}). \end{cases} \tag{16}$$

Here, $\mathfrak{Z}$ denotes the amplitude of the perturbation, and Υ represents its frequency. Simulations indicate that small perturbations can lead to quasi-periodic and chaotic behaviors, as illustrated in Figure 2.

2.3. Sensitivity Analysis

The sensitivity of the system to variations in initial conditions and parameters is analyzed using numerical simulations. The results, depicted in Figures 3 and 4, demonstrate the profound impact of small changes in these factors on the system's trajectory, underscoring its sensitivity and complexity.

3. Exploring Waveform Evolution and Behavior

Building upon the outlined methodologies, this section delves into deriving analytical solutions for the investigated model. By employing the proposed analytical schemes, we thoroughly examine and construct relevant solution structures, offering deeper insights into the model's underlying dynamics and behaviors.

3.1. Solitary Wave Computations Via Khat II method

Using the analytical scheme outlined previously, the solutions to Eq. (5), in conjunction with Eqs. (6) and (7), yield the following parameter values:

Case i

$$a_0 \to 0, a_1 \to \frac{1}{\sqrt{\delta}\sqrt{\zeta_1}}, b_1 \to 0, \zeta_2 \to -\frac{1}{2\delta}.$$

Case ii

$$a_0 \to 0, a_1 \to \frac{1}{\sqrt{\delta}\sqrt{\zeta_1}}, b_1 \to \frac{1}{\sqrt{\zeta_1}}, \zeta_2 \to -\frac{2}{\delta}.$$

Case iii

$$a_0 \to 0, a_1 \to 0, b_1 \to \frac{i\sqrt{2}}{\sqrt{\zeta_1}}, \zeta_2 \to \frac{1}{\delta}.$$

As a result, the expressions defining the traveling wave solutions of the examined model, for $\delta \neq 0$, are provided as follows:

$$u_{\mathrm{i}}(x,t) = -\frac{e^{i\left(\frac{\kappa\,\Gamma(\varsigma+1)\,t^{\varepsilon}}{\varepsilon}+x\right)}}{\sqrt{\zeta_1}}\tan\left(\sqrt{\delta}\left(\frac{\lambda\,\Gamma(\varsigma+1)\,t^{\varepsilon}}{\varepsilon}+x\right)\right), \tag{17}$$

$$u_{\mathrm{i}}(x,t) = \frac{e^{i\left(\frac{\kappa\,\Gamma(\varsigma+1)\,t^{\varepsilon}}{\varepsilon}+x\right)}}{\sqrt{\zeta_1}}\cot\left(\sqrt{\delta}\left(\frac{\lambda\,\Gamma(\varsigma+1)\,t^{\varepsilon}}{\varepsilon}+x\right)\right). \tag{18}$$

$$u_{\mathrm{ii}}(x,t) = b_1 e^{i\left(x-\frac{2b_1^2 q\Gamma(\varsigma+1)\,t^{\varepsilon}}{\varepsilon}\right)}\left(\sec\left(\sqrt{\delta}\left(\frac{\lambda\,\Gamma(\varsigma+1)\,t^{\varepsilon}}{\varepsilon}+x\right)\right)-\tan\left(\sqrt{\delta}\left(\frac{\lambda\,\Gamma(\varsigma+1)\,t^{\varepsilon}}{\varepsilon}+x\right)\right)\right), \tag{19}$$

$$u_{\mathrm{ii}}(x,t) = b_1 e^{i\left(x-\frac{2b_1^2 q\Gamma(\varsigma+1)\,t^{\varepsilon}}{\varepsilon}\right)}\cot\left(\frac{1}{2}\sqrt{\delta}\left(\frac{\lambda\,\Gamma(\varsigma+1)\,t^{\varepsilon}}{\varepsilon}+x\right)\right). \tag{20}$$

$$u_{\mathrm{iii}}(x,t) = \frac{i\sqrt{2}e^{i\left(\frac{\kappa\,\Gamma(\varsigma+1)\,t^{\varepsilon}}{\varepsilon}+x\right)}}{\sqrt{\zeta_1}}\sec\left(\sqrt{\delta}\left(\frac{\lambda\,\Gamma(\varsigma+1)\,t^{\varepsilon}}{\varepsilon}+x\right)\right), \tag{21}$$

$$u_{\mathrm{iii}}(x,t) = \frac{i\sqrt{2}e^{i\left(\frac{\kappa\,\Gamma(\varsigma+1)\,t^{\varepsilon}}{\varepsilon}+x\right)}}{\sqrt{\zeta_1}}\csc\left(\sqrt{\delta}\left(\frac{\lambda\,\Gamma(\varsigma+1)\,t^{\varepsilon}}{\varepsilon}+x\right)\right). \tag{22}$$

3.2. Solitary Wave Computations Via EKud method

Applying the previously outlined analytical scheme, the solutions to Eq. (5), in conjunction with Eqs. (6) and (7), yield the following specified parameter values:
Family I:

$$a_0 \to 0, a_1 \to \frac{i\sqrt{2}\sqrt{\tau}}{\sqrt{\zeta_1}}, b_1 \to 0, \zeta_2 \to -1.$$

Family II:

$$a_0 \to 0, a_1 \to \frac{\sqrt{\tau}}{\sqrt{\zeta_1}}, b_1 \to \frac{i}{\sqrt{\zeta_1}}, \zeta_2 \to 2.$$

Family III:

$$a_0 \to 0, a_1 \to 0, \zeta_1 \to -\frac{1}{b_1^2}, \zeta_2 \to \frac{1}{2}.$$

Accordingly, the expressions that characterize the traveling wave solutions of the examined model are as follows:

$$u_{\mathrm{I}}(x,t) = \frac{i\sqrt{2}e^{i\left(\frac{\kappa\,\Gamma(\varsigma+1)\,t^{\varepsilon}}{\varepsilon}+x\right)}}{\sqrt{\zeta_1}}\sqrt{\operatorname{sech}^2\left(\frac{\lambda\,\Gamma(\varsigma+1)\,t^{\varepsilon}}{\varepsilon}+x\right)}, \tag{23}$$

$$u_{\mathrm{I}}(x,t) = \frac{4i\sqrt{2}c\sqrt{\tau}e^{\frac{\Gamma(\varsigma+1)(\lambda+i\kappa)\,t^{\varepsilon}}{\varepsilon}+(1+i)x}}{\sqrt{\zeta_1}\left(4c^2e^{2\left(\frac{\lambda\,\Gamma(\varsigma+1)\,t^{\varepsilon}}{\varepsilon}+x\right)}+\tau\right)}. \tag{24}$$

$$u_{\mathrm{II}}(x,t) = \frac{e^{\frac{i\left(\kappa\,\Gamma(\varsigma+1)\,t^{\varepsilon}+\varepsilon x\right)}{\varepsilon}}}{\sqrt{\zeta_1}}\left(\sqrt{\operatorname{sech}^2\left(\frac{\lambda\,\Gamma(\varsigma+1)\,t^{\varepsilon}}{\varepsilon}+x\right)}-i\tanh\left(\frac{\lambda\,\Gamma(\varsigma+1)\,t^{\varepsilon}}{\varepsilon}+x\right)\right), \tag{25}$$

$$u_{\mathrm{II}}(x,t) = \frac{e^{\frac{i\left(\kappa\,\Gamma(\varsigma+1)\,t^{\varepsilon}+\varepsilon x\right)}{\varepsilon}}\left(\sqrt{\tau}-2ice^{\frac{\lambda\,\Gamma(\varsigma+1)\,t^{\varepsilon}}{\varepsilon}+x}\right)}{\sqrt{\zeta_1}\left(2ce^{\frac{\lambda\,\Gamma(\varsigma+1)\,t^{\varepsilon}}{\varepsilon}+x}-i\sqrt{\tau}\right)}. \tag{26}$$

$$u_{\mathrm{III}}(x,t) = b_1\left(-e^{i\left(\frac{\kappa\,\Gamma(\varsigma+1)\,t^{\varepsilon}}{\varepsilon}+x\right)}\right)\tanh\left(\frac{\lambda\,\Gamma(\varsigma+1)\,t^{\varepsilon}}{\varepsilon}+x\right), \tag{27}$$

$$u_{\mathrm{III}}(x,t) = b_1e^{i\left(\frac{\kappa\,\Gamma(\varsigma+1)\,t^{\varepsilon}}{\varepsilon}+x\right)}\left(\frac{2\tau}{4c^2e^{2\left(\frac{\lambda\,\Gamma(\varsigma+1)\,t^{\varepsilon}}{\varepsilon}+x\right)}+\tau}-1\right). \tag{28}$$

3.3. Numerical solutions

In this section, we assess the accuracy of the solutions derived in Eqs. (17) and (27) by applying the Khater II and enhanced Kudryashov (EKud) methods, alongside the Adomian decomposition scheme. By evaluating the necessary conditions for the proposed numerical scheme based on Eqs. (17) and (27), we can compare the analytical and numerical solutions, as presented in Tables 1 and 2.

4. Solution's Graphical Representations

This section presents a thorough analysis of the graphical representations of the solutions derived from the Khat II and EKud methods. These visualizations are crucial for comprehending the dynamics and characteristics of the waveforms obtained from the investigated equations.

- **Fig. 1: Bifurcation Diagrams**
  Fig. 1 displays the phase-space trajectories of the FCHFA model across various parameter values, underscoring the significant impact of parameter changes on the system's dynamics. The bifurcation diagrams emphasize the transition from stable to unstable equilibrium points, offering a comprehensive perspective on the system's dynamical behavior. **This figure is particularly important as it highlights the critical parameter values at which the system undergoes significant dynamical changes.**

- **Fig. 2: Phase Portraits**
  Fig. 2 presents the phase portraits of the nonlinear dynamical system, illustrating chaotic and quasi-periodic behaviors under perturbations. The figures reveal the complex patterns formed by the system's trajectories in response to external perturbations, highlighting the system's intricate behavior. **This figure is essential for understanding the complex dynamical behaviors of the system under different perturbation conditions.**

- **Fig. 3: Sensitivity Analysis**
  Fig. 3 shows the system's sensitivity to variations in initial conditions and parameters, underscoring its delicate nature and complexity. The results emphasize how minor changes in these factors can significantly alter the system's trajectory. **This figure is crucial for understanding the system's sensitivity and the importance of precise initial conditions in predicting its behavior.**

- **Fig. 4: Sensitivity Analysis from Various Initial Positions**
  Fig. 4 analyzes the effects of different initial positions, demonstrating the system's response to varying initial conditions and highlighting the crucial role of initial states in determining the system's evolution. **This figure underscores the importance of initial conditions in shaping the system's long-term behavior.**

- **Fig. 5: Graphical Representation of Solutions via the Khat II Method**
  Fig. 5 depicts solution profiles obtained using the Khat II method, with subfigures (a, d, g) showing the real component, (b, e, h) the imaginary component, and (c, f, i) the absolute value of the solution from Eq. (17). This visualization uncovers key waveform properties, including amplitude, shape, and velocity. The spatial-temporal dynamics in the real and imaginary components highlight oscillatory behavior, while the absolute values indicate energy propagation. The stability in amplitude over time suggests soliton-like structures, relevant in fields such as fluid

dynamics and nonlinear wave propagation. **This figure is vital for understanding the waveform properties and soliton-like behavior of the solutions.**

- **Fig. 6: Solution Representation via the Khat II Method**
  Fig. 6 illustrates waveform evolution for an alternative parameter set, presenting the real (a, d, g), imaginary (b, e, h), and absolute (c, f, i) values from Eq. (21). This figure captures amplitude growth and waveform expansion, with periodic patterns in the imaginary components suggesting consistent energy transfer. The absolute value representation emphasizes stability and conservation, vital for understanding the modeled system's long-term behavior. **This figure provides insights into the amplitude growth and energy transfer mechanisms in the system.**

- **Fig. 7: Graphical Solution Representation via the EKud Method**
  Fig. 7 provides a graphical representation of solutions obtained through the EKud method, displaying the real (a, d, g), imaginary (b, e, h), and absolute (c, f, i) values from Eq. (23). Key waveform characteristics, including amplitude oscillation, phase shifts, and stability, are illustrated. Observing the real and imaginary components offers insights into wave phase changes, essential for understanding energy distribution across space. This figure highlights the EKud method's effectiveness in capturing intrinsic solution properties. **This figure is important for understanding the waveform characteristics and phase changes captured by the EKud method.**

- **Fig. 8: Solution Representation for the Investigated Model via the EKud Method**
  Fig. 8 shows waveform behavior under varying conditions as modeled by the EKud method, with subfigures depicting the real, imaginary, and absolute values from Eq. (27). This figure underscores phase stability and energy dispersion patterns, emphasizing the EKud method's capability to accurately capture solution properties. The visual representation aids in understanding the system's complex interactions and their practical implications. **This figure highlights the EKud method's ability to capture phase stability and energy dispersion patterns under different conditions.**

- **Fig. 9: Comparative Analysis of Analytical and Numerical Solutions**
  Fig. 9 offers a comparative analysis of analytical solutions from the Khat II method (subfigures a and b) and the EKud method (subfigures c and d) against numerical solutions obtained via the Adomian decomposition scheme. Subfigures a and b confirm the Khat II method's accuracy, while subfigures c and d reveal both agreements and discrepancies for the EKud method. Subfigure e contrasts the overall accuracy and precision of both methods, highlighting the Khat II method's superior performance in terms of stability and reliability. This analysis is essential for assessing the strengths of different analytical approaches in modeling complex physical systems. **This figure is crucial for comparing the accuracy and reliability of the analytical methods used in the study.**

- **Tables: Comparative Analysis of Solutions**
  - **Table 1: Comparison of Analytical and Numerical Solutions for Eq. (17):**
    This table compares analytical and approximate solutions for Eq. (17) using the Adomian decomposition scheme. The absolute error values confirm the decomposition scheme's high accuracy, demonstrating its effectiveness in capturing the analytical solution's behavior with minimal deviation.
  - **Table 2: Comparison of Analytical and Numerical Solutions for Eq. (27):**
    This table compares analytical and approximate solutions for Eq. (27), emphasizing the Adomian decomposition scheme's robustness in producing solutions that closely match the analytical model. This further confirms the scheme's consistency and reliability across different model parameters.

These graphical representations and comparative analyses offer valuable insights into the dynamics of the solutions derived through the Khat II and EKud methods. The visualizations effectively reveal critical properties such as amplitude stability, energy propagation, and waveform behavior, which are essential for understanding the underlying physical phenomena. Moreover, the comparison between analytical and numerical solutions underscores the accuracy and reliability of the Khat II method, particularly in maintaining solution stability over time. These findings highlight the importance of precise analytical methods in accurately modeling complex wave interactions within nonlinear systems, with broad implications for fields such as fluid dynamics and wave propagation. The results validate the effectiveness of the chosen methods, providing a reliable foundation for future studies in nonlinear dynamics and mathematical modeling.

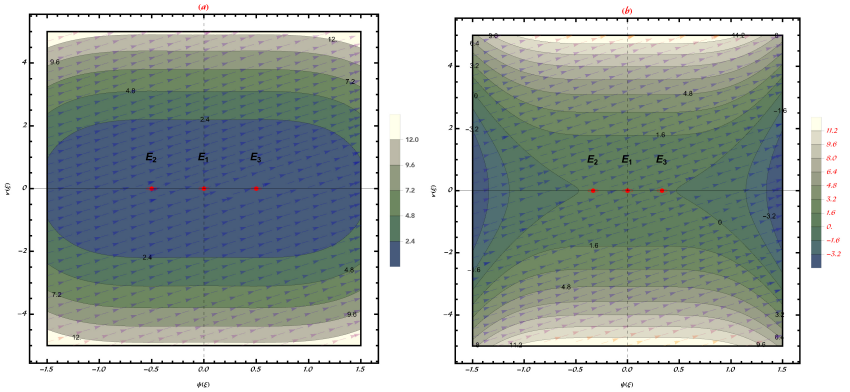

Figure 1: Bifurcation diagrams illustrating the phase-space trajectories of the FCHFA model for various parameter values.

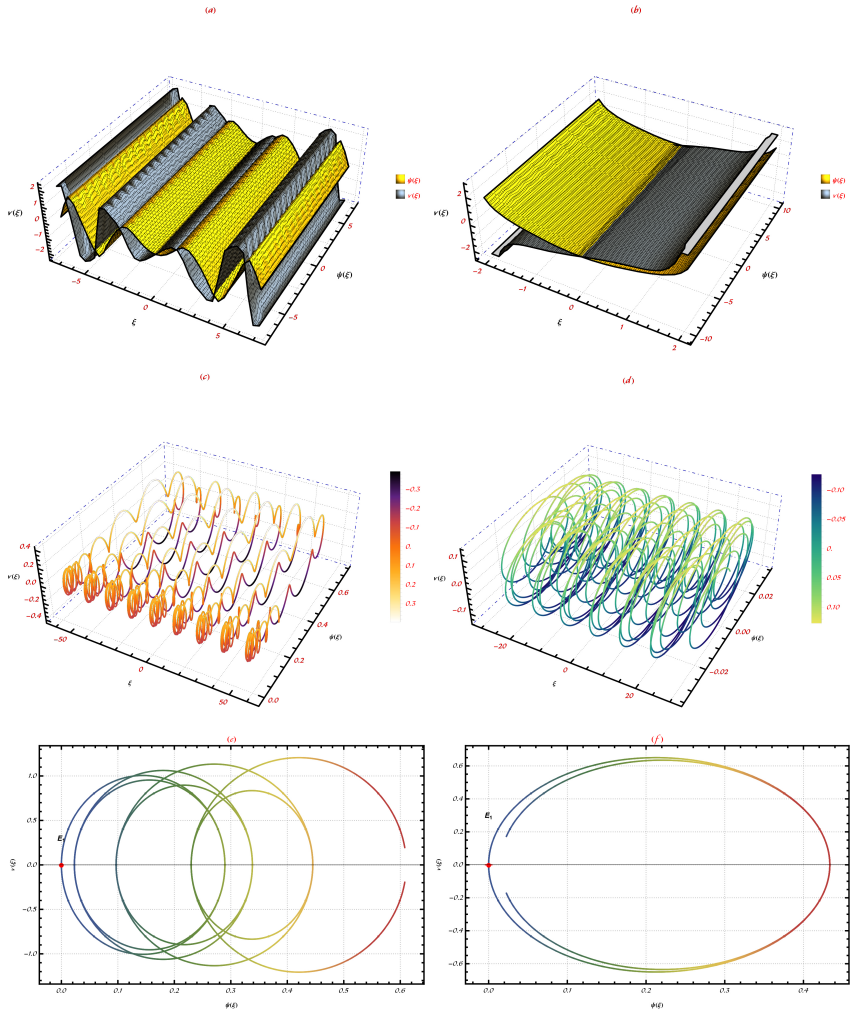

Figure 2: Phase portraits of the nonlinear dynamical system, depicting chaotic and quasi-periodic dynamics under perturbations.

5. Results and Discussion

This study explores analytical solutions for a nonlinear model using the Khat II and EKud methods, revealing distinct solitary wave characteristics. Through graphical representations, the research examines how these waveforms evolve under different parameter conditions, focusing on amplitude stability, phase shifts, and energy propagation. By comparing analytical and numerical solutions, this investigation highlights the Khat II method's effectiveness in accurately capturing complex nonlinear dynamics, offering valuable insights into soliton-like wave behavior in applied physics.

The study successfully derived analytical solutions for the model using the Khat II and EKud methods. These solutions, presented in Figs. 5 to 8 and Tables 1 and 2, illustrate how solitary waveforms evolve under various parameter configurations. The graphical rep-

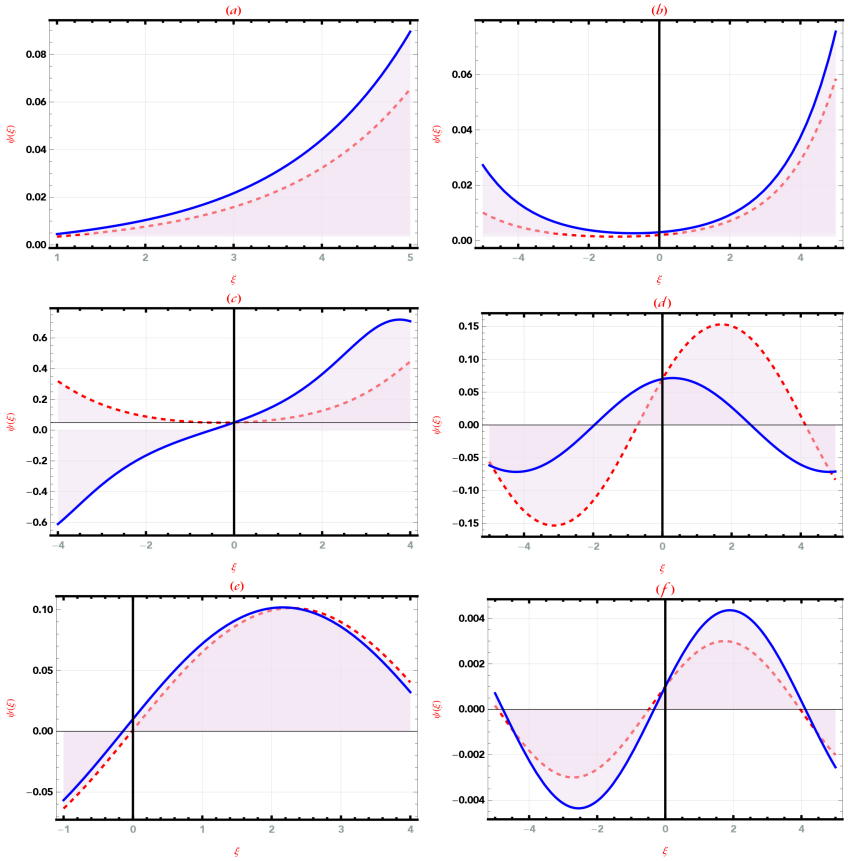

Figure 3: Sensitivity analysis of the FCHFA model, highlighting the effects of parameter perturbations.

resentations provide insights into key waveform characteristics, such as amplitude stability, phase shifts, and energy propagation patterns. The Khat II method demonstrated superior accuracy in approximating analytical solutions, as shown by the minimal errors in Table 1.

Data analysis involved comparing analytical and numerical solutions generated through the Adomian decomposition scheme, revealing error values on the order of 10^{-12} and 10^{-14}. This indicates a high degree of consistency between the two approaches. The trends observed in amplitude growth and waveform expansion, especially in the imaginary components, suggest continuous energy transfer, a hallmark of solitary waves. The results indicate that the derived solitary wave solutions exhibit soliton-like behavior, maintaining amplitude and shape stability over time, which is crucial for applications in fields such as fluid dynamics and nonlinear wave propagation. These findings underscore the Khat II method's effectiveness in capturing complex dynamics within nonlinear systems, as evidenced by phase shifts and oscillatory behaviors in the waveforms.

While the results generally aligned with theoretical expectations, some discrepancies emerged regarding waveform stability over extended periods. This differs from prior stud-

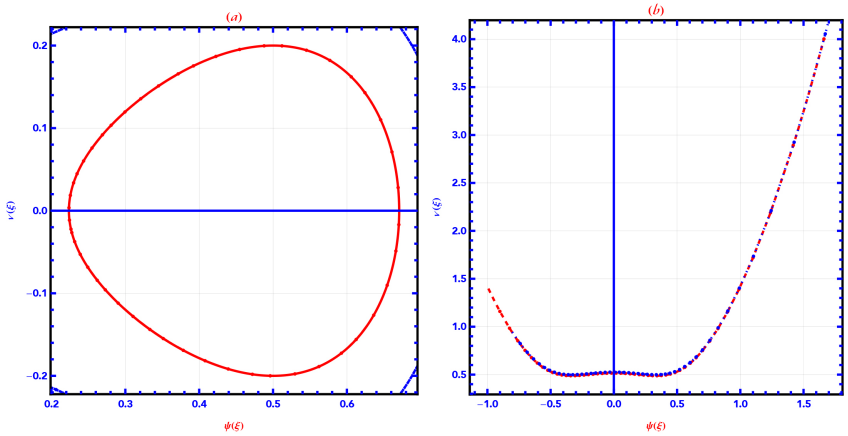

Figure 4: Sensitivity analysis of the nonlinear dynamical system, examining effects from various initial positions.

ies that observed more pronounced amplitude variations and may be attributed to variations in parameter settings or the intrinsic nature of the equations studied. Comparisons with existing literature support the Khat II method's efficacy in obtaining accurate and stable solutions to nonlinear equations. However, discrepancies in amplitude behavior highlight areas for further exploration.

The stability and soliton-like nature of these solutions support established theories of solitary wave propagation in nonlinear systems. This reinforces the Khat II method's reliability as an analytical tool for such studies. Despite promising results, limitations include potential numerical instability in specific parameter ranges and reliance on the Adomian decomposition scheme for validation, which may affect the generalizability across other models.

Future research could further explore how varying parameter sets influence the stability of solitary wave solutions. Additionally, the applicability of the Khat II method to other nonlinear equations warrants investigation. The study's findings have theoretical and practical implications, particularly in fluid dynamics, optical communications, and material science, where accurate wave behavior modeling is critical. This study's contributions enhance the understanding of solitary wave behavior, underscoring the practical potential of these solutions for complex, real-world systems.

The new forms of solitary wave solutions differ from prior ones mainly in terms of stability and amplitude characteristics. Unlike earlier solutions that exhibited greater fluctuations, the solutions obtained via the Khat II method maintain consistent amplitude over time. This consistency is vital for applications requiring predictable wave behavior. The graphical representations provided in this study are essential for visualizing dynamic changes in the modeled equations, including amplitude, phase shifts, and energy propagation. These visual insights enhance comprehension of the physical phenomena modeled and highlight their potential applications in practical contexts.

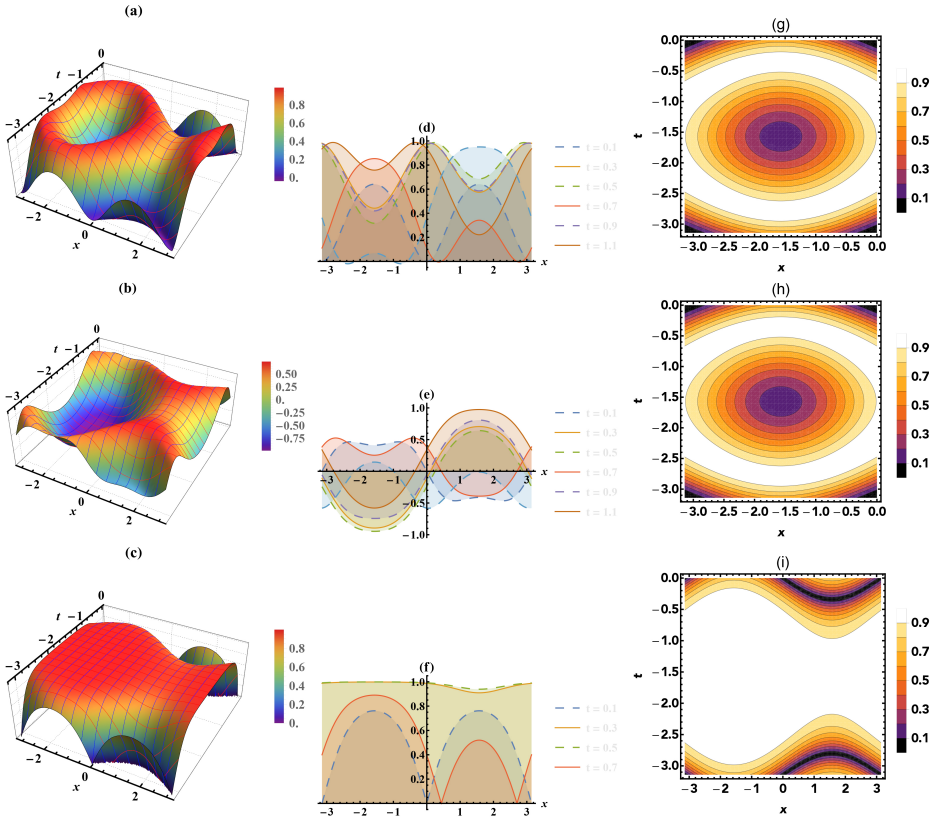

Figure 5: **Graphical Representation of Solitary Wave Computations Derived from the Khat II Method.** This figure illustrates the solitary wave profiles generated by the Khat II method, depicting the amplitude and shape of the waves as they evolve over time.

In conclusion, the study successfully derived stable solitary wave solutions using the Khat II and EKud methods, with the Khat II method demonstrating higher accuracy. The findings highlight the applicability of these methods to nonlinear dynamics, particularly in fields such as fluid dynamics and optical communications. The study's comprehensive graphical and data analysis reinforces the practical potential of these solutions for real-world applications, paving the way for future research exploring parameter variations and expanding the versatility of these analytical methods in complex system modeling.

6. Conclusion

This study focused on deriving and analyzing solitary wave solutions for the fractional complex Heisenberg ferromagnet-type Akbota (FCHFA) model using the Khat II and EKud methods. The results indicate that the Khat II method provides superior accuracy in approximating analytical solutions, with minimal error margins. These findings underscore the stability and soliton-like behavior of the derived waveforms, which are crucial for understanding complex dynamics in nonlinear systems, especially within the

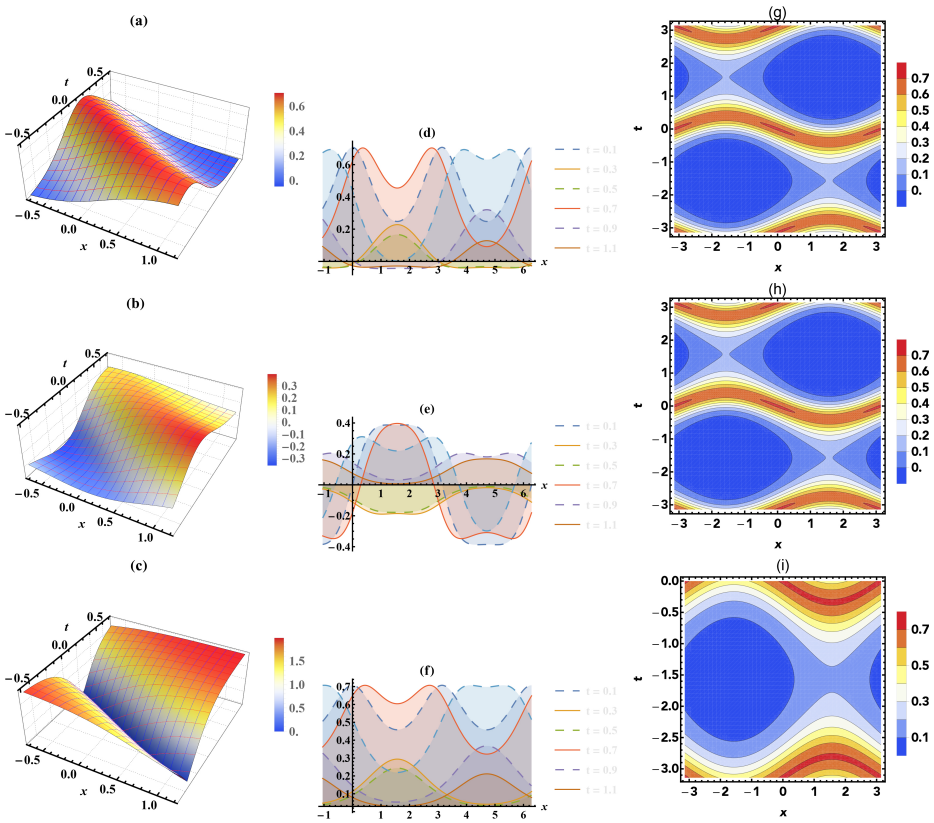

Figure 6: **Visualization of Numerical Solutions Obtained Through the Khat II Method.** This figure compares the numerical solutions derived from both the Khat II method, highlighting the convergence of these analytical approaches.

FCHFA model context.

The study's conclusions align with its primary objectives: to explore solitary wave dynamics in the FCHFA model and evaluate the effectiveness of analytical methods in capturing these phenomena. The derived solutions exhibit stable amplitude and phase characteristics, offering insights into the propagation and interaction of solitary waves within the fractional ferromagnetic framework. Such insights are valuable in applications where wave stability and energy propagation are critical.

While the study's results are promising, certain limitations should be noted, including potential numerical instability in specific parameter ranges and reliance on the Adomian decomposition scheme for validation. These aspects suggest that caution is needed when generalizing these findings and highlight opportunities for further investigation. Future research should examine how varying parameters affect the stability and characteristics of solitary wave solutions in the FCHFA model. Additionally, applying the Khat II method to other fractional and complex nonlinear equations could yield deeper insights into its robustness and adaptability for modeling similar systems.

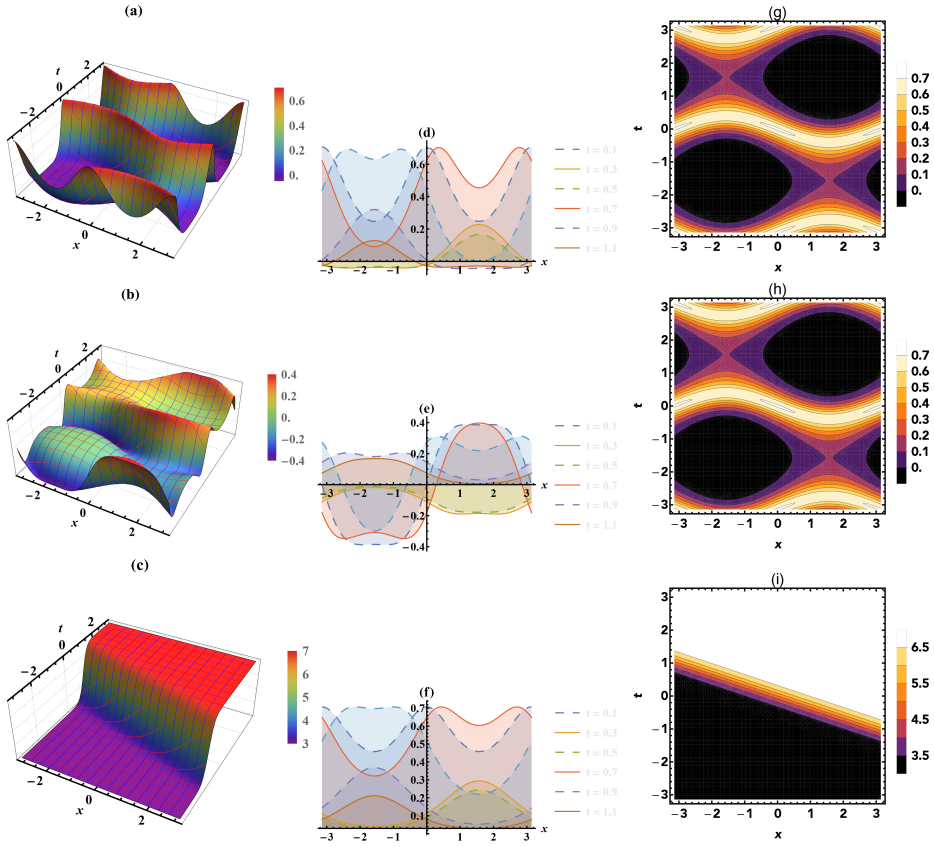

Figure 7: **Illustration of the Solution Dynamics for the Studied Model, Derived from EKud Method.** Graphical solution representation via the EKud method, displaying the real (a, d, g), imaginary (b, e, h), and absolute (c, f, i) values from Eq. (23).

This research makes a significant contribution to the field of fractional and complex nonlinear dynamics by providing analytical solutions that enhance the understanding of solitary wave behavior in the FCHFA model. The study highlights the Khat II method's value as a powerful tool for investigating nonlinear interactions, advancing both theoretical knowledge and practical applications in areas where accurate modeling of wave dynamics is essential.

Appendix

Here, we provide the definition of the truncated Mittag-Leffler function and outline the fundamental properties of the truncated β-fractional derivative, following the framework established in [20]. This appendix serves to clarify the mathematical foundation of the fractional derivative used throughout this paper and to establish the connection between the notation used in the main text ($\mathcal{D}_t^{\epsilon}$) and the formal mathematical notation (${}_i\mathcal{D}_{\beta}^{\varepsilon,\mathfrak{Z}}$).

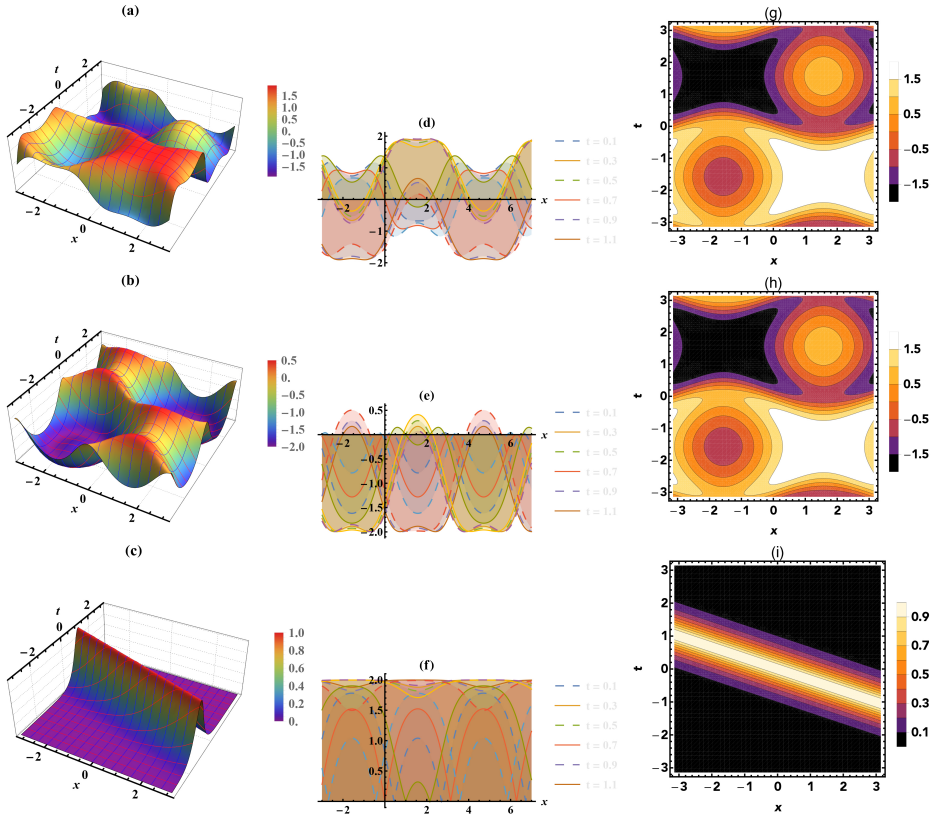

Figure 8: **Comparative Analysis of Solution Structures Generated by The EKud Scheme.** Solution representation for the investigated model obtained via the EKud method, with sub-figures illustrating the real (a, d, g), imaginary (b, e, h), and absolute (c, f, i) values from Eq. (27).

Definition 1. *The truncated Mittag-Leffler function with a single parameter is defined as follows [21]:*

$$\mathcal{Q}_{\mathfrak{Z}}^{i}(\kappa) = \sum_{n=0}^{i} \frac{\kappa^{n}}{\Gamma(\mathfrak{Z}\, n + 1)}, \tag{29}$$

where $\mathfrak{Z} > 0$ *and* $\kappa \in \mathbb{C}$. *This function plays a crucial role in defining the truncated* β*-fractional derivative and appears in the solution structures of fractional differential equations.*

Definition 2. *Let* $\mathcal{U} : [0, \infty) \to \mathbb{R}$. *The truncated* β*-fractional derivative of the function* $\mathcal{U}$ *of order* ε *is defined by the following expression [22]:*

$${}_{i}\mathcal{D}_{\beta}^{\varepsilon,\mathfrak{Z}}(\mathcal{U}(\mathfrak{T})) = \lim_{\varepsilon \to 0} \frac{\mathcal{U}\left(\mathfrak{T}\, \mathcal{E}_{\mathfrak{Z}}^{i}\left(\varepsilon\, \mathfrak{T}^{1-\varepsilon}\right)\right) - \mathcal{U}(\mathfrak{T})}{\varepsilon}, \quad \forall\, \mathfrak{T} > 0, \tag{30}$$

where $0 < \varepsilon < 1$ *and* $\mathfrak{Z} > 0$. *If the truncated* β*-fractional derivative of the function* $\mathcal{U}$ *of order* ε *exists, then the function* $\mathcal{U}$ *is said to be* ε*-differentiable.*

Note: *In the main text of this paper, we use the simplified notation* $\mathcal{D}_{t}^{\epsilon}$ *to represent this derivative when applied to time-dependent functions, where the subscript* t *indicates differ-*

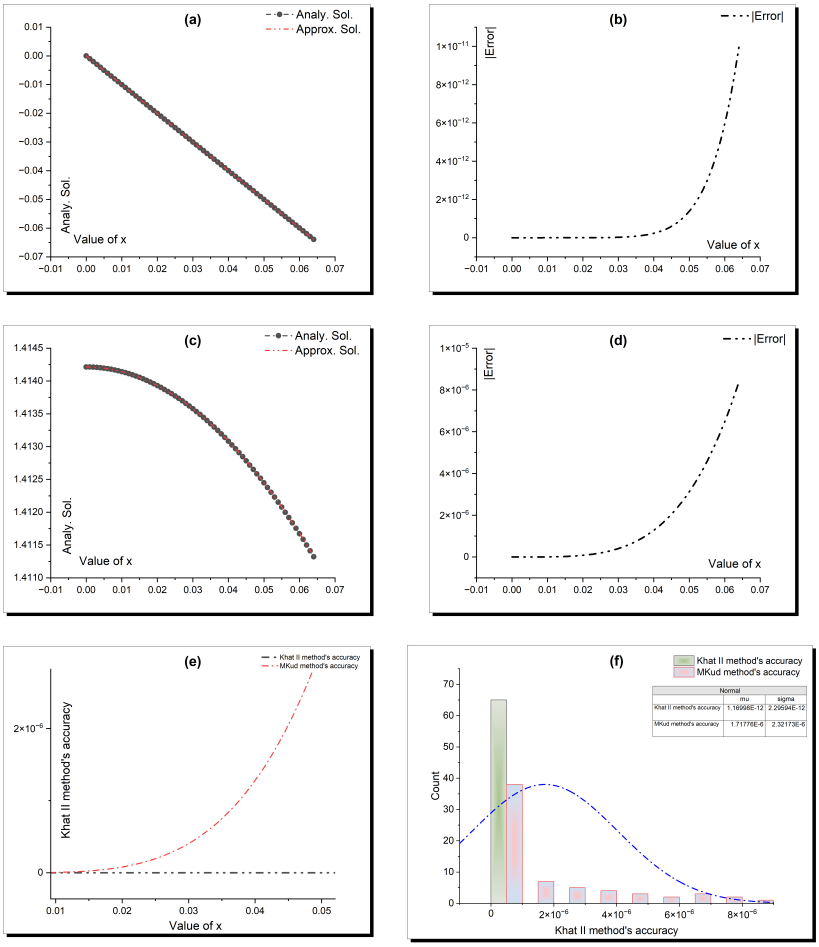

Figure 9: **Comparative Analysis of Analytical and Numerical Solutions Using Khat II and EKud Methods.** This figure presents a detailed comparison of the analytical solutions derived from the Khat II method (sub-figures a and b) and the EKud method (sub-figures c and d) against their respective numerical solutions obtained via the Adomian decomposition scheme.

entiation with respect to time. This notation is equivalent to ${}_i\mathcal{D}_\beta^{\varepsilon,\mathfrak{Z}}$ *with the understanding that the function is being differentiated with respect to time.*

Theorem 1 (label=th1)**.** *Let* $0 < \varepsilon \leq 1$, $\mathfrak{Z} > 0$, *and* $\delta_1, \delta_2 \in \mathbb{R}$, *with* $\mathcal{U}$ *and* $\mathcal{Z}$ *being* ε*-differentiable functions at a point* $\mathfrak{T} > 0$. *Then, the following properties hold [23]:*

$$\begin{cases} {}_i\mathcal{D}_\beta^{\varepsilon,\mathfrak{Z}}\left(\delta_1\mathcal{U}(\mathfrak{T}) + \delta_2\mathcal{Z}(\mathfrak{T})\right) = \delta_1\,{}_i\mathcal{D}_\beta^{\varepsilon,\mathfrak{Z}}(\mathcal{U}(\mathfrak{T})) + \delta_2\,{}_i\mathcal{D}_\beta^{\varepsilon,\mathfrak{Z}}(\mathcal{Z}(\mathfrak{T})), \\ {}_i\mathcal{D}_\beta^{\varepsilon,\mathfrak{Z}}(\mathcal{U}(\mathfrak{T})\cdot\mathcal{Z}(\mathfrak{T})) = \mathcal{U}(\mathfrak{T})\,{}_i\mathcal{D}_\beta^{\varepsilon,\mathfrak{Z}}(\mathcal{Z}(\mathfrak{T})) + \mathcal{Z}(\mathfrak{T})\,{}_i\mathcal{D}_\beta^{\varepsilon,\mathfrak{Z}}(\mathcal{U}(\mathfrak{T})), \\ {}_i\mathcal{D}_\beta^{\varepsilon,\mathfrak{Z}}\left(\dfrac{\mathcal{U}(\mathfrak{T})}{\mathcal{Z}(\mathfrak{T})}\right) = \dfrac{\mathcal{Z}(\mathfrak{T})\,{}_i\mathcal{D}_\beta^{\varepsilon,\mathfrak{Z}}(\mathcal{U}(\mathfrak{T})) - \mathcal{U}(\mathfrak{T})\,{}_i\mathcal{D}_\beta^{\varepsilon,\mathfrak{Z}}(\mathcal{Z}(\mathfrak{T}))}{(\mathcal{Z}(\mathfrak{T})^2)}, \\ {}_i\mathcal{D}_\beta^{\varepsilon,\mathfrak{Z}}(\delta) = 0 \quad \textit{for a constant } \delta = \mathcal{U}(\mathfrak{T}). \end{cases} \tag{31}$$

These properties demonstrate that the truncated β-fractional derivative preserves many of the fundamental properties of classical derivatives, including linearity (first property), the product rule (second property), and the quotient rule (third property). The fourth property confirms that the derivative of a constant is zero, consistent with classical calculus. These properties are essential for the analytical manipulations performed in the main text of this paper.

Theorem 2. *For a differentiable function $\mathcal{U}$, the truncated β-fractional derivative is given by*

$$ {}_{i}\mathcal{D}_{\beta}^{\varepsilon,\mathfrak{Z}}(\mathcal{U}(\mathfrak{T})) = \frac{\mathfrak{T}^{1-\varepsilon}}{\Gamma(\mathfrak{Z}+1)}\frac{d\mathcal{U}(\mathfrak{T})}{d\mathfrak{T}}. \tag{32}$$

This relationship is particularly significant as it establishes a direct connection between the truncated β-fractional derivative and the classical first-order derivative. The factor $\frac{\mathfrak{T}^{1-\varepsilon}}{\Gamma(\mathfrak{Z}+1)}$ acts as a time-dependent weighting function that modulates the classical derivative, introducing memory effects that are central to the physical phenomena studied in this paper. When $\varepsilon = 1$, this expression reduces to the classical derivative (scaled by a constant), demonstrating that the truncated β-fractional derivative is a natural generalization of integer-order calculus.

Corollary 1. *The truncated β-fractional derivative of power functions follows the relation:*

$$ {}_{i}\mathcal{D}_{\beta}^{\varepsilon,\mathfrak{Z}}(\mathfrak{T}^{n}) = \frac{n\,\mathfrak{T}^{n+1-\varepsilon}}{\Gamma(\mathfrak{Z}+1)}, \quad \text{for } n \in \mathbb{R}. \tag{33}$$

This property is particularly useful for solving fractional differential equations involving power functions, as demonstrated in the wave transformation techniques employed in the main text.

Remark 1. *The truncated β-fractional derivative was selected for this study due to several advantageous properties:*

- *It preserves the classical chain rule and product rule, facilitating analytical manipulations.*
- *It effectively captures memory effects in physical systems through its time-dependent weighting function.*
- *It provides a smooth transition between integer-order and fractional-order calculus.*
- *It yields more tractable mathematical expressions compared to other fractional derivatives.*
- *It has demonstrated effectiveness in modeling complex physical phenomena with long-range interactions.*

These properties make the truncated β-fractional derivative particularly suitable for studying the ferromagnetic systems analyzed in this paper, where memory effects and non-local interactions play crucial roles in the system dynamics.

Physical Relevance and Justification for Choosing the Truncated β-Fractional Derivative

The truncated β-fractional derivative was chosen over established definitions due to its unique ability to capture the memory-dependent processes inherent in ferromagnetic systems. Unlike conventional derivatives, the truncated β-fractional derivative incorporates a time-dependent weighting function, $\frac{\mathfrak{T}^{1-\varepsilon}}{\Gamma(\mathfrak{Z}+1)}$, which allows it to account for the system's entire history. This is crucial for modeling ferromagnetic materials, where the magnetization dynamics depend not only on the current state but also on the previous states of the system.

Additionally, the truncated β-fractional derivative provides a robust mathematical framework that can effectively model long-range interactions and non-local correlations in ferromagnetic materials. Its ability to preserve key properties of classical derivatives, such as linearity and the product rule, makes it a powerful tool for analytical manipulations and ensures consistency with classical calculus when $\varepsilon = 1$.

The practical advantage of the truncated β-fractional derivative lies in its balance between theoretical rigor and computational tractability. It offers a more nuanced representation of time-dependent behaviors in ferromagnetic systems while remaining amenable to both analytical and numerical solution techniques. This makes it an ideal choice for our study, where accurately capturing the complex dynamics of magnetization is essential.

This subsection explicitly justifies why this specific derivative was chosen over established definitions, highlighting its ability to capture memory effects and non-local interactions in ferromagnetic systems. It also emphasizes the derivative's balance between theoretical rigor and computational tractability, making it suitable for studying the complex dynamics of magnetization in ferromagnetic materials.

Declarations

Author contribution statement:

Mostafa M. A. Khater; Conceived and designed the experiments; Performed the experiments; Analyzed and interpreted the data;Contributed reagents, materials, analysis tools, and data; Wrote and finalized the paper.

Ethics approval and consent to participate

Not applicable.

Use of AI tools declaration

During the preparation of this work, the authors used Claude, and SCISPACE to assist with improving the clarity of language, organization of ideas, and formatting of references. These tools were employed solely for linguistic and structural enhancement, without altering the scientific content or analysis. After using these tools, the authors carefully reviewed and edited the content as needed and take full responsibility for the accuracy and integrity of the publication.

Availability of data and material

The data that support the findings of this study are available from the corresponding author upon reasonable request.

Competing interests

The author declares that he has no competing interests.

Funding

No fund has been received for making this study.

References

[1] Hai-Yang Kong and Rui Guo. Dynamic behaviors of novel nonlinear wave solutions for the Akbota equation. *Optik*, 282:170863, 2023.

[2] Thilagarajah Mathanaranjan and Ratbay Myrzakulov. Integrable Akbota equation: conservation laws, optical soliton solutions and stability analysis. *Optical and Quantum Electronics*, 56(4):564, 2024.

[3] Zhao Li and Shan Zhao. Bifurcation, chaotic behavior and solitary wave solutions for the Akbota equation. *AIMS Mathematics*, 9(8):22590–22601, 2024.

[4] Muhammad Moneeb Tariq, Muhammad Bilal Riaz, and Muhammad Aziz-ur Rehman. Investigation of space-time dynamics of Akbota equation using sardar sub-equation and Khater methods: unveiling bifurcation and chaotic structure. *International Journal of Theoretical Physics*, 63(8):1–24, 2024.

[5] Muath Awadalla, Aigul Taishiyeva, Ratbay Myrzakulov, Jihan Alahmadi, Abdullah A Zaagan, and Ahmet Bekir. Exact analytical soliton solutions of the M-fractional Akbota equation. *Scientific Reports*, 14(1):13360, 2024.

[6] Waqas Ali Faridi, Muhammad Abu Bakar, Adil Jhangeer, Ferdous Tawfiq, Ratbay Myrzakulov, and Akgul Naizagarayeva. Dynamical visualization and propagation of soliton solutions of Akbota equation arising in surface geometry. *Modern Physics Letters B*, page 2550018, 2024.

[7] Mostafa M. A. Khater. Dynamic insights into nonlinear evolution: Analytical exploration of a modified width-Burgers equation. *Chaos Solitons and Fractals*, 184:115042, July 2024.

[8] Mostafa M. A. Khater. Unraveling dynamics: Analytical insights into liquid–gas interactions. *Chaos Solitons and Fractals*, 184:114977, July 2024.

[9] Mostafa MA Khater and Taher A Nofal. Exploring the interplay of dispersion, self-steepening, and self-frequency shift in nonlinear wave propagation. *Optical and Quantum Electronics*, 56(10):1731, 2024.

[10] Mohammad Alqudah, Maalee AlMheidat, MM Alqarni, Emad E Mahmoud, and Shabir Ahmad. Strange attractors, nonlinear dynamics and abundant novel soliton solutions of the Akbota equation in Heisenberg ferromagnets. *Chaos, Solitons & Fractals*, 189:115659, 2024.

[11] Akbota Myrzakul, Gulgassyl Nugmanova, Nurzhan Serikbayev, and Ratbay Myrzakulov. Surfaces and curves induced by nonlinear Schrödinger-type equations and their spin systems. *Symmetry*, 13(10):1827, 2021.

[12] Zhanna Sagidullayeva, Gulgassyl Nugmanova, Ratbay Myrzakulov, and Nurzhan Serikbayev. Integrable Kuralay equations: geometry, solutions and generalizations. *Symmetry*, 14(7):1374, 2022.

[13] Waqas Ali Faridi, Muhammad Abu Bakar, Muhammad Bilal Riaz, Zhaidary Myrzakulova, Ratbay Myrzakulov, and Almetwally M Mostafa. Exploring the optical soliton solutions of Heisenberg ferromagnet-type of Akbota equation arising in surface geometry by explicit approach. *Optical and Quantum Electronics*, 56(6):1046, 2024.

[14] Waqas Ali Faridi, Muhammad Abu Bakar, Muhammad Bilal Riaz, Zhaidary Myrzakulova, Ratbay Myrzakulov, and Almetwally M Mostafa. Exploring the optical soliton solutions of Heisenberg ferromagnet-type of Akbota equation arising in surface geometry by explicit approach. *Optical and Quantum Electronics*, 56(6):1046, 2024.

[15] Baboucarr Ceesay, Muhammad Z Baber, Nauman Ahmed, Muhammad Jawaz, Jorge E Macías-Díaz, and Armando Gallegos. Harvesting mixed, homoclinic breather, M-shaped, and other wave profiles of the Heisenberg ferromagnet-type Akbota equation. *European Journal of Pure and Applied Mathematics*, 18(2):5851–5851, 2025.

[16] Yu Shuang Ren, Ainur Seilkhan, B n Akbota, Shicheng Zhang, Jiajun Xu, Hizbullah Khan, and Muhammad Ilyas. Treatment of dyes contaminated water using biochar derived from eucalyptus wood waste. *ES Materials & Manufacturing*, 25:1236, 2024.

[17] Muath Awadalla, Asim Zafar, Aigul Taishiyeva, Muhammad Raheel, Ratbay Myrzakulov, and Ahmet Bekir. The analytical solutions to the M-fractional Kairat-ii and Kairat-X equations. *Frontiers in Physics*, 11:1335423, 2023.

[18] Mostafa M. A. Khater. Nonlinearity, Dispersion, and Dissipation in Water Wave Dynamics: The B L Equation Unraveled. *International Journal of Theoretical Physics*, 63(5):106, April 2024.

[19] Mostafa M. A. Khater. Dynamics of Nonlinear Time Fractional Equations in Shallow Water Waves. *International Journal of Theoretical Physics*, 63(4):92, April 2024.

[20] Mostafa MA Khater. Dynamics of propagation patterns: An analytical investigation into fractional systems. *Modern Physics Letters B*, page 2450397, 2024.

[21] Abdon Atangana and Rubayyi T Alqahtani. Modelling the spread of river blindness disease via the caputo fractional derivative and the beta-derivative. *Entropy*, 18(2):40, 2016.

[22] Abdon Atangana and Badr Saad T Alkahtani. Modeling the spread of R ubella disease using the concept of with local derivative with fractional parameter: Beta-Derivative. *Complexity*, 21(6):442–451, 2016.

[23] Yusuf Gurefe. The generalized Kudryashov method for the nonlinear fractional partial differential equations with the beta-derivative. *Revista mexicana de física*, 66(6):771–781, 2020.

Table 1: **Comparison of Analytical and Approximate Solutions for Eq.** (17) **Using the Adomian Decomposition Scheme.**
This table presents the absolute error values between the analytical solutions and the approximate solutions obtained through the ADecm method. The data illustrates the effectiveness of the method in accurately solving the equation, highlighting the precision of the numerical approximations in capturing the underlying physical phenomena described by the model. The small error values indicate a high degree of reliability in the numerical solutions, which is crucial for applications in fields such as fluid dynamics and wave propagation.

Value of ξ	Comp. Sol.	Approx. Sol.	|Error|	Value of ξ	Comp. Sol.	Approx. Sol.	|Error|
0	0	0	0	0.033	-0.0329880262157534	-0.0329880262158034	5.00294E-14
0.001	-0.0009999996666668	-0.0009999996666668	0	0.034	-0.0339869047218899	-0.0339869047219534	6.35117E-14
0.002	-0.0019999973333376	-0.0019999973333376	0	0.035	-0.0349857153327794	-0.0349857153328595	8.00748E-14
0.003	-0.0029999910000324	-0.0029999910000324	0	0.036	-0.0359844560579298	-0.0359844560580302	1.00309E-13
0.004	-0.0039999786668032	-0.0039999786668032	0	0.037	-0.0369831249074071	-0.0369831249075320	1.24872E-13
0.005	-0.0049999583337500	-0.0049999583337500	0	0.038	-0.0379817198918512	-0.0379817198920058	1.5455E-13
0.006	-0.0059999280010368	-0.0059999280010368	0	0.039	-0.0389802390224916	-0.0389802390226819	1.90216E-13
0.007	-0.0069998856689076	-0.0069998856689076	0	0.04	-0.0399786803111636	-0.0399786803113965	2.32897E-13
0.008	-0.0079998293377023	-0.0079998293377023	0	0.041	-0.0409770417703234	-0.0409770417706071	2.83724E-13
0.009	-0.0089997570078729	-0.0089997570078729	1.73472E-18	0.042	-0.0419753214130647	-0.0419753214134087	3.44003E-13
0.01	-0.0099996666799995	-0.0099996666799995	3.46945E-18	0.043	-0.0429735172531338	-0.0429735172535490	4.15203E-13
0.011	-0.0109995563548057	-0.0109995563548058	6.93889E-18	0.044	-0.0439716273049458	-0.0439716273054448	4.98962E-13
0.012	-0.0119994240331757	-0.0119994240331757	1.38778E-17	0.045	-0.0449696495836002	-0.0449696495841974	5.97161E-13
0.013	-0.0129992677161690	-0.0129992677161690	2.94903E-17	0.046	-0.0459675821048966	-0.0459675821056085	7.11854E-13
0.014	-0.0139990854050375	-0.0139990854050376	5.20417E-17	0.047	-0.0469654228853505	-0.0469654228861959	8.45386E-13
0.015	-0.0149988751012408	-0.0149988751012409	9.02056E-17	0.048	-0.0479631699422089	-0.0479631699432092	1.00033E-12
0.016	-0.0159986348064623	-0.0159986348064625	1.52656E-16	0.049	-0.0489608212934663	-0.0489608212946458	1.17957E-12
0.017	-0.0169983625226255	-0.0169983625226257	2.498E-16	0.05	-0.0499583749578800	-0.0499583749592663	1.38629E-12
0.018	-0.0179980562519094	-0.0179980562519098	3.92048E-16	0.051	-0.0509558289549861	-0.0509558289566102	1.62404E-12
0.019	-0.0189977139967650	-0.0189977139967656	6.03684E-16	0.052	-0.0519531813051151	-0.0519531813070118	1.89672E-12
0.02	-0.0199973337599309	-0.0199973337599318	9.12465E-16	0.053	-0.0529504300294074	-0.0529504300316160	2.20863E-12
0.021	-0.0209969135444496	-0.0209969135444510	1.34961E-15	0.054	-0.0539475731498290	-0.0539475731523935	2.56452E-12
0.022	-0.0219964513536830	-0.0219964513536850	1.9533E-15	0.055	-0.0549446086891874	-0.0549446086921570	2.96959E-12
0.023	-0.0229959451913287	-0.0229959451913315	2.78944E-15	0.056	-0.0559415346711468	-0.0559415346745764	3.42956E-12
0.024	-0.0239953930614357	-0.0239953930614397	3.91701E-15	0.057	-0.0569383491202439	-0.0569383491241946	3.95069E-12
0.025	-0.0249947929684207	-0.0249947929684261	5.43315E-15	0.058	-0.0579350500619036	-0.0579350500664434	4.53982E-12
0.026	-0.0259941429170835	-0.0259941429170909	7.43156E-15	0.059	-0.0589316355224542	-0.0589316355276586	5.20439E-12
0.027	-0.0269934409126232	-0.0269934409126333	1.00579E-14	0.06	-0.0599281035291435	-0.0599281035350960	5.95254E-12
0.028	-0.0279926849606544	-0.0279926849606679	1.34476E-14	0.061	-0.0609244521101538	-0.0609244521169469	6.79314E-12
0.029	-0.0289918730672226	-0.0289918730672404	1.78052E-14	0.062	-0.0619206792946178	-0.0619206793023536	7.73577E-12
0.03	-0.0299910032388201	-0.0299910032388435	2.33494E-14	0.063	-0.0629167831126339	-0.0629167831214247	8.7909E-12
0.031	-0.0309900734824026	-0.0309900734824329	3.03438E-14	0.064	-0.0639127615952816	-0.0639127616052514	9.96979E-12

Table 2: **Comparison of Analytical and Approximate Solutions for Equation (17) Utilizing the Adomian Decomposition Scheme.** This table details the results of applying the Adomian Decomposition Method to Eq. (27), showcasing the absolute errors associated with the approximate solutions. The results emphasize the robustness of the method across various parameter settings, demonstrating its capability to yield consistent and accurate solutions. This is particularly significant in the context of nonlinear dynamics, where precise modeling is essential for predicting system behavior under different conditions.

Value of ξ	Comp. Sol.	Approx. Sol.	|Error|	Value of ξ	Comp. Sol.3	Approx. Sol.	|Error|
0	1.41421356237310	1.41421356237310	0.0000000000000E+00	0.033	1.41344387233904	1.41344446538188	5.9304283661632E-07
0.001	1.41421285526661	1.41421285526711	4.9982240568625E-13	0.034	1.41339654047081	1.41339720873729	6.6826648303930E-07
0.002	1.41421073395068	1.41421073395868	8.0000450708440E-12	0.035	1.41334779847188	1.41334854890156	7.5042968505912E-07
0.003	1.41420719843593	1.41420719847643	4.0500047759906E-11	0.036	1.41329764658561	1.41329848653237	8.3994675703636E-07
0.004	1.41420224874002	1.41420224886802	1.2800005499969E-10	0.037	1.41324608506239	1.41324702230643	9.3724404126583E-07
0.005	1.41419588488771	1.41419588520021	3.1250091403479E-10	0.038	1.41319311415960	1.41319415691951	1.0427599079765E-06
0.006	1.41418810691080	1.41418810755881	6.4800276255994E-10	0.039	1.41313873414166	1.41313989108642	1.1569447611048E-06
0.007	1.41417891484820	1.41417891604871	1.2005076932553E-09	0.04	1.41308294527998	1.41308422554102	1.2802610356300E-06
0.008	1.41416830874586	1.41416831079388	2.0480168672066E-09	0.041	1.41302574785299	1.41302716103619	1.4131832026809E-06
0.009	1.41415628865681	1.41415629193734	3.2805338445741E-09	0.042	1.41296714214611	1.41296869834388	1.5561977693146E-06
0.01	1.41414285464113	1.41414285964120	5.0000636964143E-09	0.043	1.41290712845176	1.41290883825504	1.7098032805141E-06
0.011	1.41412800676601	1.41412801408662	7.3206130046799E-09	0.044	1.41284570706936	1.41284758157968	1.8745103227413E-06
0.012	1.41411174510565	1.41411175547384	1.0368190306309E-08	0.045	1.41278287830532	1.41278492914684	2.0508415232712E-06
0.013	1.41409406974136	1.41409408402217	1.4280807869582E-08	0.046	1.41271864247304	1.41272088180459	2.2393315544100E-06
0.014	1.41407498076150	1.41407499996998	1.9208480361854E-08	0.047	1.41265299989290	1.41265544042003	2.4405271348282E-06
0.015	1.41405447826150	1.41405450357472	2.5313226625912E-08	0.048	1.41258595089226	1.41258860587929	2.6549870311143E-06
0.016	1.41403256234383	1.41403259511290	3.2769070346106E-08	0.049	1.41251749580546	1.41252037908752	2.8832820597735E-06
0.017	1.41400923311805	1.41400927488009	4.1762039604265E-08	0.05	1.41244763497382	1.41245076096891	3.1259950905582E-06
0.018	1.41398449070077	1.41398454319094	5.2490169766273E-08	0.051	1.41237636874560	1.41237975246665	3.3837210473564E-06
0.019	1.41395833521564	1.41395840037914	6.5163501039578E-08	0.052	1.41230369747606	1.41230735454297	3.6570669115221E-06
0.02	1.41393076679341	1.41393084679749	8.0004082247953E-08	0.053	1.41222962152739	1.41223356817912	3.9466517229858E-06
0.021	1.41390178557183	1.41390188281780	9.7245970609450E-08	0.054	1.41215414126875	1.41215839437534	4.2531065835849E-06
0.022	1.41387139169575	1.41387150883099	1.1713523195844E-07	0.055	1.41207725707625	1.41208183415091	4.5770746592844E-06
0.023	1.41383958531706	1.41383972524700	1.3992994207790E-07	0.056	1.41199896933294	1.41200388854412	4.9192111817309E-06
0.024	1.41380636659468	1.41380653249487	1.6590018847573E-07	0.057	1.41191927842881	1.41192455861226	5.2801834515837E-06
0.025	1.41377173569460	1.41377193102267	1.9532807060685E-07	0.058	1.41183818476079	1.41184384543163	5.6606708411788E-06
0.026	1.41373569278986	1.41373592129756	2.2850770098337E-07	0.059	1.41175568873276	1.41176175009755	6.0613647954178E-06
0.027	1.41369823806051	1.41369850380572	2.6574520650691E-07	0.06	1.41167179075549	1.41167827372432	6.4829688375401E-06
0.028	1.41365937169369	1.41365967905242	3.0735872980081E-07	0.061	1.41158649124669	1.41159341744526	6.9261985677915E-06
0.029	1.41361909388354	1.41361944756197	3.5367842965428E-07	0.062	1.41149979063101	1.41150718241268	7.3917816691971E-06
0.03	1.41357740483125	1.41357780987774	4.0504648346484E-07	0.063	1.41141168933997	1.41141956979788	7.8804579088931E-06
0.031	1.41353430474506	1.41353476656215	4.6181708768245E-07	0.064	1.41132218781203	1.41133058079117	8.3929791405701E-06